

# Spectrum Analysis of Wind Profiling Radar Measurements

RUAN Zheng<sup>1\*</sup> (阮 征), MU Ruiqi<sup>2</sup> (慕瑞琪), WEI Ming<sup>2</sup> (魏 鸣), and GE Runsheng<sup>1</sup> (葛润生)

<sup>1</sup> State Key Laboratory of Severe Weather, Chinese Academy of Meteorological Sciences, Beijing 100081

<sup>2</sup> Nanjing University of Information Science & Technology, Nanjing 210044

(Received November 12, 2013; in final form May 19, 2014)

## ABSTRACT

Unlike previous studies on wind turbulence spectrum in the planetary boundary layer, this investigation focuses on high-altitude (1–5 km) wind energy spectrum and turbulence spectrum under various weather conditions. A fast Fourier transform (FFT) is used to calculate the wind energy and turbulence spectrum density at high altitudes (1–5 km) based on wind profiling radar (WPR) measurements. The turbulence spectrum under stable weather conditions at high altitudes is expressed in powers within a frequency range of  $2 \times 10^{-5}$ – $10^{-3} \text{ s}^{-1}$ , and the slope  $b$  is between  $-0.82$  and  $-1.04$ , indicating that the turbulence is in the transition from the energetic area to the inertial sub-range. The features of strong weather are reflected less obviously in the wind energy spectrum than in the turbulence spectrum, with peaks showing up at different heights in the latter spectrum. Cold windy weather appears over a period of 1.5 days in the turbulence spectrum. Wide-range rainstorms exhibit two or three peaks in the spectrum over a period of 15–20 h, while in severe convective weather conditions, there are two peaks at 13 and 9 h. The results indicate that spectrum analysis of wind profiling radar measurements can be used as a supplemental and helpful method for weather analysis.

**Key words:** wind profiling radar, wind energy spectrum, turbulence spectrum

**Citation:** Ruan Zheng, Mu Ruiqi, Wei Ming, et al., 2014: Spectrum analysis of wind profiling radar measurements. *J. Meteor. Res.*, **28**(4), 656–667, doi: 10.1007/s13351-014-3171-y.

## 1. Introduction

Wind measurements can be analyzed by using two methods associated with Fourier transforms. The time-domain method studies energy changes with time, while the frequency-domain method studies the distribution of energy with frequency.

Panofsky (1955) and Griffith et al. (1956) employed the power-spectrum density analysis to study the spectral characteristics of boundary layer wind. Van der Hoven (1957) performed a power-spectrum analysis of horizontal wind over a wide range of frequencies. These studies showed that there appears to be two major eddy-energy peaks in the spectrum: one peak at a period of 4 days and the other at a period of 1 min. Between the two peaks, a broad spectral gap is centered at a frequency ranging from 1 to 10 cycles per hour (Atkinson, 1981). Since the 1970s, spectrum

analysis has been applied in boundary layer turbulence studies (Endlich et al., 1969; Bowne and Ball, 1970; Kaimal et al., 1972). Højstrup (1981) developed a distribution model of the turbulence spectrum in neutral and unstable stratification, and this has since been widely used. Panofsky et al. (1982) showed that the distribution of turbulence spectrum varies for different topographies. Recently, Chellali et al. (2010) proposed that the features of turbulence spectrum are affected by topography and spatial location.

In-depth research has been carried out on turbulence spectrum analysis, mainly in boundary layer wind measurements. Zhang et al. (1987) used observations of horizontal wind speed from a 320-m meteorological tower to analyze the spectral characteristics and vertical distribution of turbulence in the boundary layer, and concluded that in the atmosphere, under both stable and unstable stratification, there are sev-

Supported by the National Natural Science Foundation of China (41075023 and 41475029), China Meteorological Administration Special Public Welfare Research Fund (GYHY201306004), and Key Technology Integration and Application Fund of the China Meteorological Administration (CMAGJ2013M74).

\*Corresponding author: ruanz@cams.cma.gov.cn.

eral cycles at a period of a few minutes to 10 minutes. Bian et al. (2002) discovered that the turbulence spectrum characteristics of the boundary layer are consistent with Kolmogorov's "−5/3 rate," (Kolmogorov, 1941a, b) and confirmed that the power exponent and exponent function are more appropriate. Wang and Mao (2004) used wavelets to analyze the turbulence spectrum characteristics of a convective  $\beta$ -scale weather system. Spectral analysis has also been applied to cold windy weather (Luo and Zhu, 1993; Liu and Hong, 1996; Tian et al., 2011) and cold fronts (Zhao et al., 1982; Sun and Xu, 1997).

Due to the absence of refined wind measurements, analysis of the energy spectrum and turbulence spectrum in the atmospheric layer above the boundary layer is limited. By applying wind profile radar (WPR) in atmospheric soundings (Liu et al., 2003), it is possible to obtain high-altitude wind data on a continuous basis. Research on the energy spectrum and turbulence spectrum based on high-reliability WPR measurements at altitudes of 1–5 km has thus been developed (Wang et al., 2007; Wei and Zhang, 2009; Sun et al., 2012; Yu, 2012). This study aims to provide a statistical analysis of wind energy and turbulence spectrum at 1–5-km heights under various weather conditions.

## 2. Method

Spectral analysis, which is expressed by frequency or wavenumber, is a statistical tool to study signal properties. The Parseval equation is as follows:

$$\begin{aligned} \int_{-\infty}^{\infty} x^2(t)dt &= \frac{1}{2\pi} \int_{-\infty}^{\infty} |F(\omega)|^2 d\omega \\ &= \int_{-\infty}^{\infty} |F(f)|^2 df, \end{aligned} \quad (1)$$

where  $\omega$  is the angular frequency and  $f$  is the frequency. Then,  $S(\omega) = |F(\omega)|^2$ , where  $S(\omega)$  is the energy spectrum density, indicating the contribution fluctuation makes to the total energy.

The energy spectrum density estimates are calculated by using the Fourier transform. The autocorrelation function is defined as

$$R(\tau) = \int_{-\infty}^{\infty} f(t)f^*(t-\tau)dt, \quad (2)$$

where  $f(t) = \frac{1}{2\pi} \int_{-\infty}^{\infty} F(\omega)e^{i\omega t}d\omega$  and the Fourier transform of the autocorrelation function is

$$\begin{aligned} R(\tau) &= \frac{1}{2\pi} \int_{-\infty}^{\infty} |F(\omega)|^2 e^{i\omega\tau} d\omega \\ &= \int_{-\infty}^{\infty} |F(f)|^2 e^{i2\pi f\tau} df, \end{aligned} \quad (3)$$

in which  $S(f) = |F(f)|^2$ .

The energy spectrum density estimate is

$$S(f) = \int_{-\infty}^{\infty} R(\tau)e^{-i2\pi f\tau} d\tau. \quad (4)$$

To reduce the leakage effect caused by the Fourier transform, an appropriate window should be chosen.

### 2.1 Wind energy spectrum analysis

In this study, the horizontal wind-speed data used in the wind energy spectrum analysis are obtained from WPR measurements. The autocorrelation function of the time-domain data  $V_h(t)$  is

$$R_{V_h}(\tau) = \int_{-\infty}^{\infty} V_h(t)V_h^*(t-\tau)dt, \quad (5)$$

and the Fourier transform for the autocorrelation function is the unit volume energy spectrum density,

$$S_{V_h}(f) = \int_{-\infty}^{\infty} \rho V_h(t)V_h(t-\tau)e^{-i2\pi\tau t}d\tau, \quad (6)$$

where the unit of frequency  $f$  is  $s^{-1}$ , the unit of air density  $\rho$  is  $kg\ m^{-3}$ , and the unit of horizontal wind speed  $V_h$  is  $m\ s^{-1}$ . The change of air density with height must be considered in the wind energy spectrum analysis of high-altitude wind data. Let  $S_{V_h}(f)$  be the energy density of horizontal wind speed, it can be calculated as  $\rho V_h^2$  s; then, the unit of the unit volume energy spectrum density can be given as  $(kg\ m^{-3})(m^2\ s^{-1})$ .

The wind energy spectra are used to characterize the variation of the wind energy density with frequency, and they are considered to be related to various weather systems.

### 2.2 Turbulence spectrum analysis

Irregular fluctuation is the basic characteristic of turbulence. Horizontal wind can be calculated as

$V_h = \bar{V}_h + u'$ , where  $\bar{V}_h$  is the mean wind and  $u'$  is the fluctuation. The Fourier transform of the autocorrelation function of  $u'$  is the turbulent energy spectral density.

According to Kolmogorov's theory (Kolmogorov, 1941a, b), the inertial sub-range is a turbulence region where the Reynolds number is large enough to meet local homogeneous isotropic conditions, so its turbulence characteristics only depend on the dissipation rate. The energy spectral function is defined by

$$E(k) = C\varepsilon^{2/3}k^{-5/3}, \quad (7)$$

where  $k$  is the wavenumber,  $\varepsilon$  is the turbulence dissipation rate, and  $C$  is a constant. The function is called the “ $-5/3$  law.” The inertial sub-range of the turbulence energy spectrum can also be expressed by frequency (Sheng et al., 2003):

$$S(f) = C_1\varepsilon^{2/3}f^{-5/3}, \quad (8)$$

where  $S(f)$  is the turbulence spectrum density. The turbulence spectrum analysis using wind tower observations shows that the slope of the turbulence spectrum at frequencies between  $10^{-2}$  and  $10^2$  is  $-5/3$  in the inertial sub-range (Bian et al., 2002).

Figure 1 shows the turbulence spectrum changes with wave number (Tian et al., 2011). The spectrum can be divided into five ranges: the dissipation range, the inertial sub-range, the energy range, the largest vortex range, and the large eddy range. The energy range produces turbulent energy, which can neither be generated nor be dissipated but is transferred to smaller scales of motion in the inertial sub-range or changed into internal energy because of the viscosity of the fluid molecules in the dissipative range. In the inertial sub-range, the slope of the turbulence spectrum is  $-5/3$ , which is steeper than the slope in the energy range but shallower than in the dissipation range (Kaimal and Finnigan, 1994). The turbulence spectrum density is normalized as:  $S'_{u'} = S_{u'}/\sigma_{u'}^2$ , where  $\sigma_{u'}^2$  expresses the variance of wind fluctuation.

### 2.3 The trend in the turbulence spectrum

The average wind data are usually treated as the mean wind for data collected over a short period. However, the mean wind for wind data collected over long

periods changes with time, and is called the trend. The fluctuation of the wind is obtained by using the least-square curve fitting to calculate the trend and deduct it from the wind data. Figure 2 shows the turbulence spectrum with two different methods used for the mean wind calculation. In Fig. 2a, the average wind data are treated as the mean wind and in Fig. 2b the trend is calculated as the mean wind. The data are on 23 June 2011. Figure 2b shows a more distinct 28-h eddy energy.

## 3. Equipment and data processing

### 3.1 Instruments

The horizontal wind-speed data used in the spectral analysis are obtained from CFL-08 troposphere wind profiler radar, which is located at Yanqing, Beijing ( $40.45^\circ\text{N}$ ,  $115.96^\circ\text{E}$ ; 487.90-m elevation). Table 1 summarizes the main properties of the radar. Rigorous calibration and standardization were carried out on the wind profile radar. Compared with air sounding, the accuracy of the wind profile radar corresponds with the specification. Deng et al. (2012) evaluated the detection accuracy of the radar using observations in 2010.

### 3.2 Data processing

The wind profile radar provides horizontal wind-speed data and signal-to-noise ratio (SNR), echo intensity, spectral width, and so on. The data were ob-

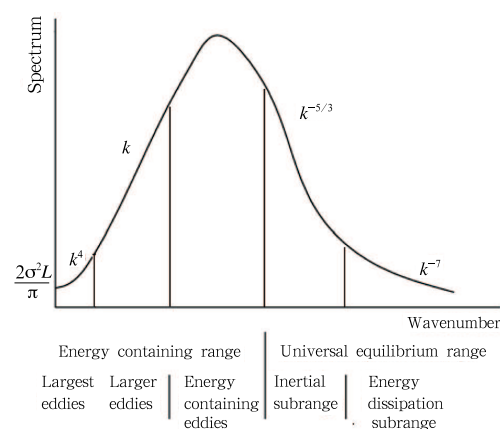


**Fig. 1.** Turbulence spectrum changes with wavenumber. (From Tian et al., 2011)

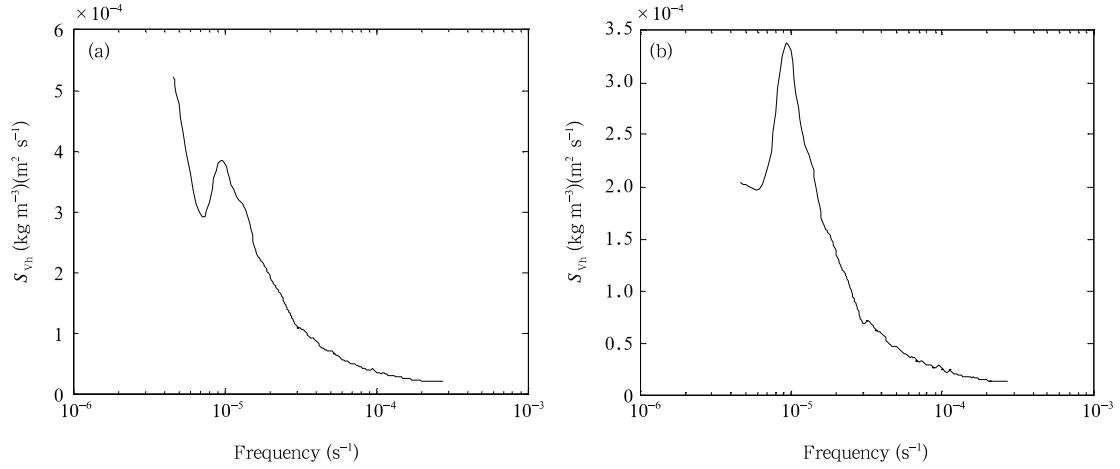


**Fig. 2.** The turbulent spectra obtained with mean wind derived differently. (a) Average as mean wind and (b) trend as mean wind.

**Table 1.** Parameters of the CFL-08 (troposphere II) wind profiling radar

Parameter	Value
Wavelength (mm)	674
Antennae shape	Phased array
Antenna section (m <sup>2</sup> )	9×9
Beamwidth (°)	4
Antenna gain (dB)	29
Scan patterns	Five beams (vertical direction and four range distances from the zenith of 14°)
Peak transmitter power (kW)	7.7
Minimum detectable power of receiver (dBm)	< -140
Coherent integration	50
FFT count	512
Minimum detection level (m)	240
Maximum detection level (m)	12030
Range resolution (m)	240
Anemometry accuracy	Wind speed < 1 m s <sup>-1</sup> , wind direction < 10°

tained from December 2010 to October 2012, at a sampling interval of 6 min. Quality control was applied as follows. Wind data that had an SNR of less than -15 dB were removed from the energy spectrum analysis because of their inaccuracy. Data series that had five consecutive missing data points were rejected. When individual missing data occurred in the data sequence, neighboring data were used to fill the gap by using linear interpolation.

According to the duration of different disastrous weather events, the data length chosen for cold windy

weather and summer rainstorms is 7 days, while 3 days is chosen for severe convective weather. The trend is identified in the turbulence spectrum density calculation. Data used for the turbulence spectrum features of the stable weather analysis are detected every 6 min for a period of 24 h.

#### 4. Characteristics of turbulence spectrum at high altitude

To examine the characteristics of the turbulence spectrum at high altitude, 10 sets of wind data under stable weather conditions are chosen. The data period is 24 h and the frequency range is from  $10^{-5}$  to  $10^{-2}$  s<sup>-1</sup>. Figure 3 shows the normalized turbulence spectrum on 28 January 2011 at an altitude of 1110 m. The abscissa is frequency and the ordinate is normalized turbulence spectrum density. Logarithmic coordinates have been used.

Figure 3 shows that the distribution of the turbulence spectrum is linear. By using least-square linear fitting, the turbulence spectrum density in the frequency range  $2 \times 10^{-5}$ – $10^{-3}$  s<sup>-1</sup> can be expressed as

$$S(f) = af^b, \quad (9)$$

where  $a$  is the intercept of the abscissa, which is related to the turbulence dissipation rate; and  $b$  is the slope. The parameters of the turbulence spectrum for Fig. 3 are  $a = 9 \times 10^{-4}$ ,  $b = -0.93$ , and the fitting

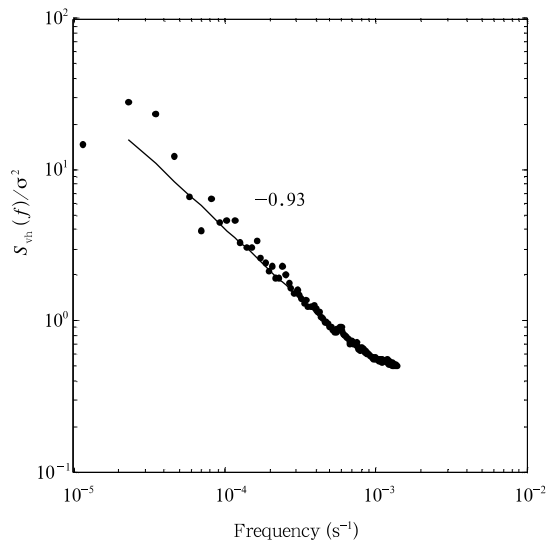


**Fig. 3.** Turbulence spectrum features on 28 January 2011.

rate is 0.99.

Table 2 summarizes the values of  $a$  and  $b$  for the turbulence spectrum of the 10 sets of data under stable weather conditions at different heights:  $a$  varies

from  $4 \times 10^{-4}$  to  $4 \times 10^{-3}$  and  $b$  varies from  $-0.82$  to  $-1.04$ , which is less than the value  $(-5/3)$  in the inertial sub-range. The turbulence spectrum distributes in power in the frequency ranges of  $2 \times 10^{-5} - 10^{-3} \text{ s}^{-1}$  at heights between 1000 and 5000 m;  $b$  is less than  $-5/3$ , showing that the turbulence is in the energy region that is transiting to the inertial sub-range.

The turbulence spectrum density of horizontal wind speed and its two orthogonal components  $u$  and  $v$  have been calculated. Figure 4 shows the turbulence spectrum of the horizontal wind speed,  $V_h$ ,  $u$ , and  $v$  on 1 December 2012 at an altitude of 1110 m. The results indicate that the three variables have a characteristic in common. The slope  $b$  is  $-0.96$ ,  $-0.97$ , and  $-0.97$ , in the frequency range of  $2 \times 10^{-5} - 10^{-3} \text{ s}^{-1}$ . It can then be concluded that the distribution of the turbulence spectrum in stable weather cases does not depend on the wind direction.

However, the situation is different for rainy days. Figure 5 shows the distributions of the turbulence

**Table 2.** Values of the turbulence spectrum parameters  $a$  and  $b$  and the fitting rate  $R$  under stable weather cases

Height Time	1110 m			2190 m			3150 m			4110 m			5070 m		
	$a$	$b$	$R$												
December 6, 2010	$1 \times 10^{-3}$	-0.91	0.99	$1 \times 10^{-3}$	-0.96	0.98	$9 \times 10^{-4}$	-0.97	0.99	$4 \times 10^{-3}$	-1.03	0.80	$3 \times 10^{-3}$	-0.86	0.80
December 9, 2010	$1 \times 10^{-3}$	-0.87	0.99	$7 \times 10^{-4}$	-0.96	0.92	$4 \times 10^{-4}$	-1.02	0.99	$7 \times 10^{-4}$	-0.96	0.99	$4 \times 10^{-3}$	-0.80	0.92
January 28, 2011	$9 \times 10^{-4}$	-0.93	0.96	$4 \times 10^{-4}$	-1.04	0.98	$8 \times 10^{-4}$	-0.94	0.92	$2 \times 10^{-3}$	-0.87	0.97	$7 \times 10^{-4}$	-0.99	0.86
December 11, 2011	$1 \times 10^{-3}$	-0.89	0.89	$9 \times 10^{-4}$	-0.96	0.91	$1 \times 10^{-3}$	-0.92	0.80	$1 \times 10^{-3}$	-0.88	0.98	$3 \times 10^{-3}$	-0.93	0.87
December 26, 2011	$1 \times 10^{-3}$	-0.90	0.96	$7 \times 10^{-4}$	-0.94	0.99	$1 \times 10^{-3}$	-0.91	0.99	$1 \times 10^{-3}$	-0.92	0.96	$1 \times 10^{-3}$	-0.88	0.99
July 4, 2012	$1 \times 10^{-3}$	-0.86	0.95	$5 \times 10^{-4}$	-0.95	0.93	$2 \times 10^{-3}$	-0.84	0.84	$1 \times 10^{-3}$	-0.94	0.94	$1 \times 10^{-3}$	-0.90	0.80
October 2, 2012	$1 \times 10^{-3}$	-0.93	0.92	$6 \times 10^{-4}$	-0.97	0.99	$1 \times 10^{-3}$	-0.86	0.92	$1 \times 10^{-3}$	-0.94	0.96	$8 \times 10^{-4}$	-0.92	0.98
October 3, 2012	$2 \times 10^{-3}$	-0.82	0.99	$1 \times 10^{-3}$	-0.90	0.99	$3 \times 10^{-3}$	-0.82	0.93	$3 \times 10^{-3}$	-0.84	0.88	$1 \times 10^{-3}$	-0.89	0.94
December 1, 2012	$6 \times 10^{-4}$	-0.97	0.99	$1 \times 10^{-3}$	-0.88	0.97	$7 \times 10^{-4}$	0.98	0.85	$4 \times 10^{-4}$	-1.03	0.99	$5 \times 10^{-4}$	-0.98	0.99
December 6, 2012	$2 \times 10^{-3}$	-0.86	0.96	$6 \times 10^{-4}$	-0.98	0.97	$8 \times 10^{-4}$	-0.91	0.99	$1 \times 10^{-3}$	-0.91	0.98	$1 \times 10^{-3}$	-0.91	0.99

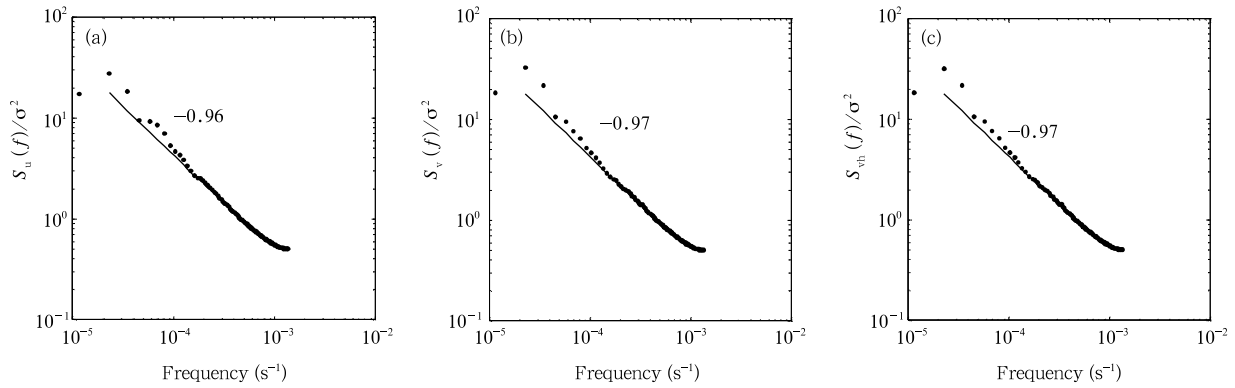


**Fig. 4.** Turbulence spectrum features of different variables at 1110-m height under stable weather on 1 December 2012. (a)  $u$ , (b)  $v$ , and (c)  $V_h$ .

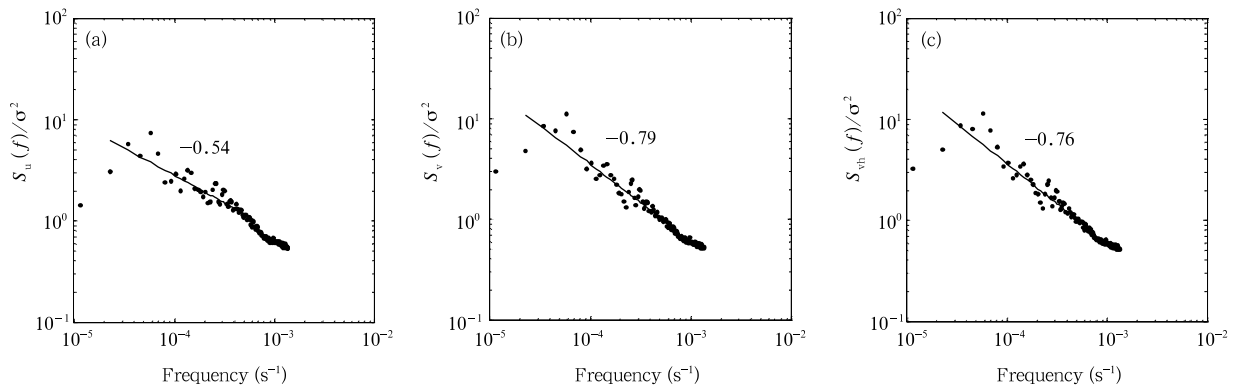


**Fig. 5.** Turbulence spectrum features of different variables at 1110-m height under rainy weather on 3 June 2012. (a)  $u$ , (b)  $v$ , and (c)  $V_h$ .

spectrum for different variables at an altitude of 1110 m in severe convective weather cases at 0000–2400 BT (Beijing Time) 3 June 2012. The slope  $b$  is  $-0.54$ ,  $-0.79$ , and  $-0.76$ , which are quite different to those for stable weather cases.

## 5. Spectrum characteristics in various weather conditions

### 5.1 Wind energy spectrum under stable weather conditions

The wind energy spectrum in stable weather conditions is calculated as follows. The observations from 0000 BT 5 to 2400 BT 11 December 2010, and 0000 BT 3 to 2400 BT 5 July 2010 are chosen as typical examples of winter and summer weather conditions. Figure 6 shows that there is no peak during these periods, and the distribution of energy spectrum in the

whole frequency band is relatively flat. The energy spectrum density decreases with increasing frequency. Figure 6 also shows that at the same height, the wind energy spectrum density in summer is nearly one order of magnitude smaller than in winter. The value decreases homogeneously with the reducing height in winter, while in summer it is dense in the altitude range of 1000–2000 m. The distribution of the spectrum in the two seasons is similar, as is the normalized turbulence spectrum in stable weather cases.

Table 3 gives a summary of the spectral density of horizontal wind at five heights in stable weather. As the height reduces from 5000 to 1000 m, the wind energy spectrum density decreases by one order of magnitude in winter, which is the same as that shown in Fig. 6. In summer, the spectral density decreases by half. Overall, the spectral density change with height is greater in winter than in summer.

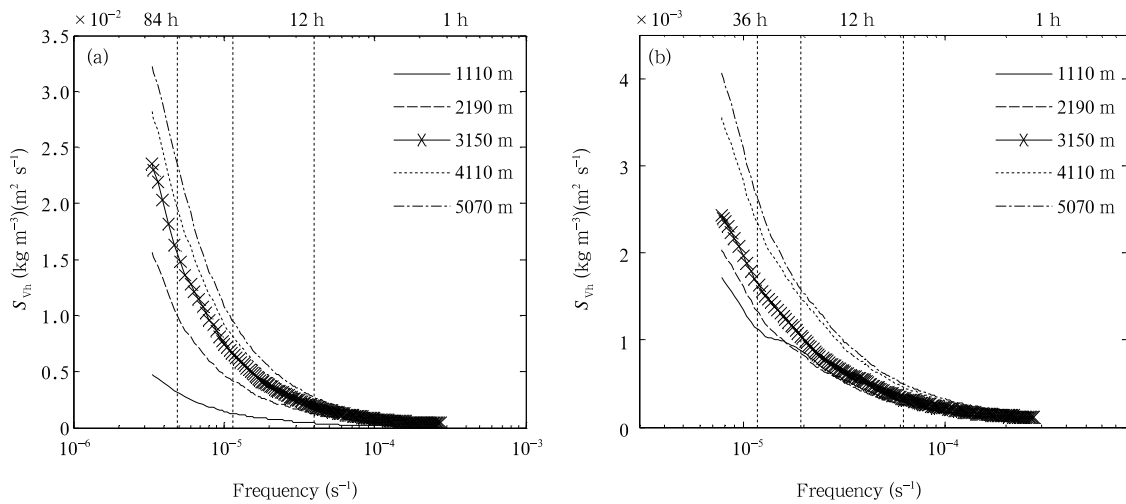


**Fig. 6.** Wind energy spectrum features for stable weather cases. (a) 5–11 December 2012 and (b) 3–5 July 2010.

**Table 3.** Spectral density of horizontal wind at five heights in stable weather

Sampling time	Height (m)	Wind energy spectrum density ((kg m <sup>-3</sup> ) (m <sup>2</sup> s <sup>-1</sup> ))			Ratio of turbulent spectrum density to wind energy spectrum density (%)		
		Frequency	Frequency	Frequency	Frequency	Frequency	Frequency
		1	2	3	1	2	3
Winter (0000 BT 5 to 2400 BT 11 December 2010)	5070	2.3×10 <sup>-2</sup>	3.0×10 <sup>-3</sup>	2.7×10 <sup>-3</sup>	0.9	3.4	3.7
	4110	1.9×10 <sup>-2</sup>	8.0×10 <sup>-3</sup>	2.3×10 <sup>-3</sup>	0.6	2.7	2.5
	3150	1.5×10 <sup>-2</sup>	6.5×10 <sup>-3</sup>	1.9×10 <sup>-3</sup>	0.4	2.4	2.7
	2190	9.5×10 <sup>-3</sup>	4.2×10 <sup>-3</sup>	1.3×10 <sup>-3</sup>	0.4	4.4	6.0
	1110	3.0×10 <sup>-3</sup>	1.3×10 <sup>-3</sup>	4.3×10 <sup>-4</sup>	1.7	7.2	11.3
Summer (0000 BT 3 to 2400 BT 5 July 2010)	5070	2.5×10 <sup>-3</sup>	1.5×10 <sup>-3</sup>	5.0×10 <sup>-4</sup>	1.1	3.8	6.0
	4110	2.3×10 <sup>-3</sup>	1.5×10 <sup>-3</sup>	4.6×10 <sup>-4</sup>	1.3	5.3	8.0
	3150	1.6×10 <sup>-3</sup>	1.0×10 <sup>-3</sup>	3.2×10 <sup>-4</sup>	1.0	10.6	7.5
	2190	1.3×10 <sup>-3</sup>	8.4×10 <sup>-4</sup>	2.5×10 <sup>-4</sup>	1.5	10.5	9.6
	1110	1.2×10 <sup>-3</sup>	8.7×10 <sup>-4</sup>	2.9×10 <sup>-4</sup>	1.6	23.0	25.9

The turbulence spectrum density accounting for the proportion of wind energy spectrum density increases with frequency, as shown in Table 3. As the height reduces, the ratio becomes greater as well, and this characteristic is more obvious in summer.

**5.2 Spectrum characteristics of cold windy weather**

The data used in the spectrum analysis of cold windy weather are from the Beijing wind profile radar. The sampling interval is 30 min and the data period is 7 days. On 11 November 2012, winds at level 5 or 6 were observed in Beijing; in some local areas, winds even reached level 7, and then weakened to level 3 at night with significant cooling. Figure 7a shows the

horizontal wind speed below the altitude of 5000 m, Fig. 7b shows the wind energy spectrum, and Fig. 7c shows the turbulence spectrum, for this cold windy weather. The five curves represent the spectrum density at 5070, 4110, 3150, 2190, and 1110 m.

The different appearance of the wind energy spectrum for cold windy and stable weather in winter can be seen in Fig. 7b. At the altitude range of 5070–2190 m, the energy spectrum density only changes a little, while it decreases rapidly in the range of 2190–1110 m. This is different from the changes in stable weather. In the turbulence spectrum (Fig. 7c), compared with the stable weather, there is a clear peak at the frequency  $3.0 \times 10^{-5} \text{ s}^{-1}$ . The intensity of the peak gradually decreases from 5070 to 2190 m.

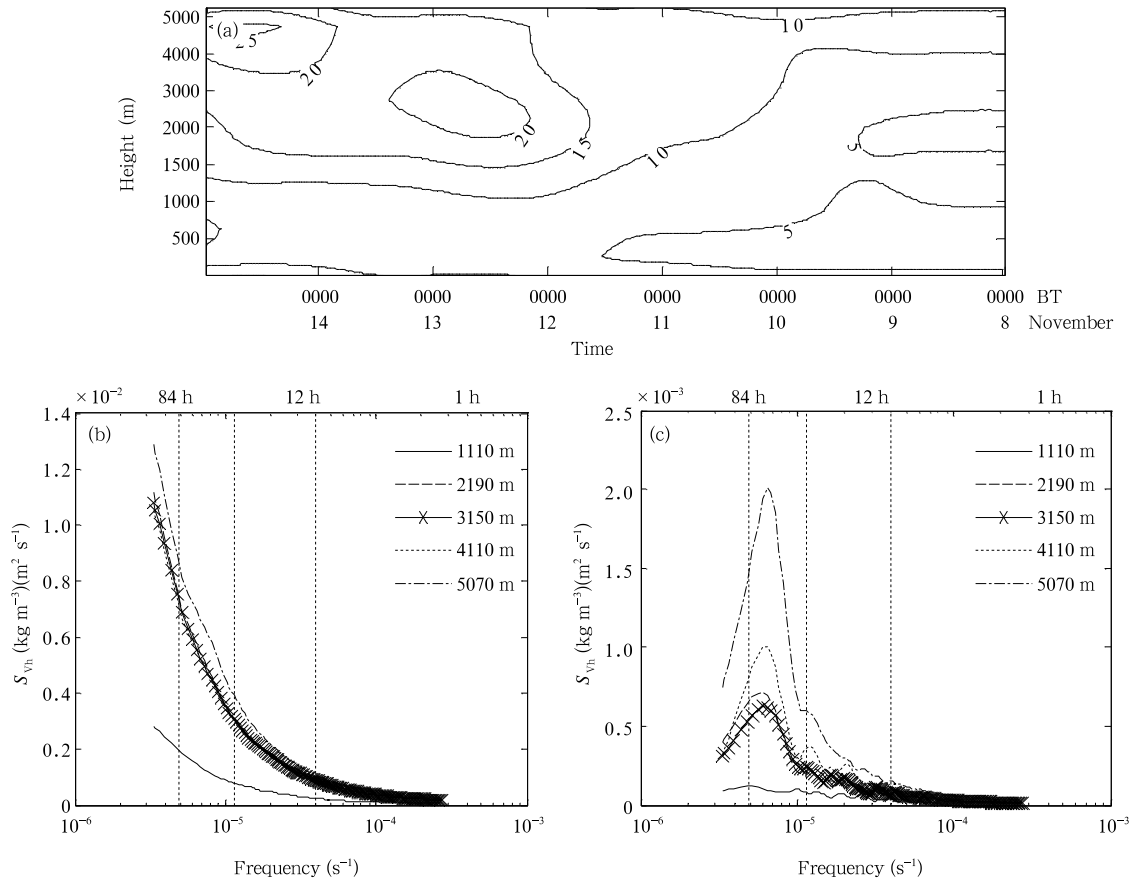


**Fig. 7.** (a) Horizontal wind speed, (b) wind energy spectrum of horizontal wind, and (c) turbulent spectrum of horizontal wind, under cold windy weather during 8–14 November 2012.

Table 4 gives the spectral density of horizontal wind at five heights in cold windy weather. There appears to be a transmission of the energy spectrum density from high to low altitudes. From 5070 to 2190 m, the energy spectrum density decreases quickly and then increases slowly. In the peak area, the turbulence spectrum density accounting for the proportion of the wind energy spectrum density increases rapidly; the higher the height, the higher the proportion. The ra-

tios at the five heights are 22.4%, 12.8%, 9.6%, 8.8%, and 7.3%, respectively.

Table 4 and Fig. 7 show that there is a period of 1.5 days in cold windy weather where the wind energy spectrum from 5070 to 2190 m decreases quickly and then increases slowly. A strong wind shear caused the intense turbulence. The amplitude in the peak area at high altitude is greater than at the lower levels. This may be due to the energy passing from the upper air

**Table 4.** Spectral density of horizontal wind at five heights in cold windy weather

Sampling time	Height (m)	Energy spectrum density ( $kg\ m^{-3})(m^2\ s^{-1})$ )			Ratio of turbulence spectrum density to wind energy spectrum density (%)		
		Frequency	Frequency	Frequency	Frequency	Frequency	Frequency
		1	2	3	1	2	3
8–14 November 2012	5070	$8.0 \times 10^{-3}$	$3.9 \times 10^{-3}$	$1.1 \times 10^{-3}$	2.1	22.4	12.5
	4110	$6.7 \times 10^{-3}$	$3.0 \times 10^{-3}$	$8.9 \times 10^{-4}$	1.5	12.8	11.0
	3150	$6.9 \times 10^{-3}$	$3.0 \times 10^{-3}$	$8.9 \times 10^{-4}$	0.9	9.6	8.7
	2190	$7.0 \times 10^{-3}$	$3.0 \times 10^{-3}$	$8.9 \times 10^{-4}$	0.8	8.8	7.4
	1110	$1.9 \times 10^{-3}$	$7.7 \times 10^{-4}$	$2.6 \times 10^{-4}$	0.6	7.3	12.5

to the lower levels.

### 5.3 Spectrum characteristics of summer rainstorms

Compared with the stable weather, the turbulence spectrum during summer rainstorms has several peaks. This is the turbulence characteristics of the mesoscale rainstorm weather. On 23 June 2011, heavy rain fell in the Beijing area; total 24-h rainfall reached 241 mm. The rainstorm was sudden and intense. It had an uneven spatial distribution and significant mesoscale characteristics. The precipitation was concentrated in the period 16–19 h, with many areas experiencing instantaneous hail. Figure 8a shows the horizontal wind speed below the altitude of 5000 m from 0000 BT 20 to 2400 BT 26 June 2011. Figures 8b and 8c show the wind energy spectrum and the turbulence spectrum for this rainstorm.

The wind energy spectrum (Fig. 8b) shows that the amplitude decreases as the height reduces. In contrast to the spectrum in cold windy weather, the wind energy spectrum becomes more stable with height, and the slope of the wind energy spectrum decreases with decreasing height. The spectrum density is only 20% of that in cold windy weather at the same altitude. There are 2–3 peaks at different heights in Fig. 8c. The peaks are located in the frequency range of  $7 \times 10^{-6}$ – $2 \times 10^{-5} \text{ s}^{-1}$ , and have a period of about 1 day. It can be seen that at 1110 m, there are two peaks located at  $5 \times 10^{-6}$  and  $2 \times 10^{-5} \text{ s}^{-1}$ , while there are no peaks at 2190 m.

Table 5 gives the spectral density of horizontal wind at five heights in the summer rainstorm case. The characteristic of spectral density changing with height is similar to that in stable weather. The turbulence spectrum density accounting for the proportion of wind energy spectrum density significantly increases

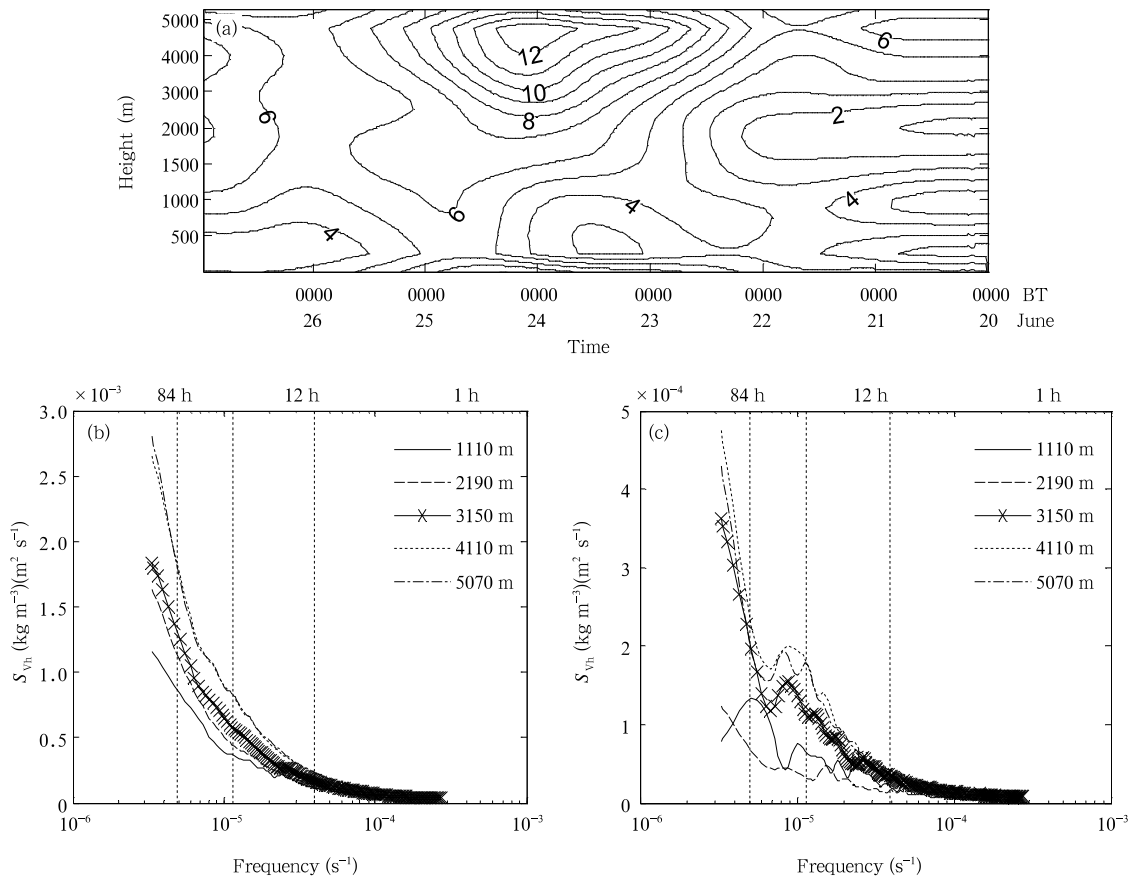


Fig. 8. As in Fig. 7, but for summer rainstorms during 8–14 June 2011.

**Table 5.** Spectral density of horizontal wind at five heights in the summer rainstorm case

Sampling time	Height (m)	Wind energy spectrum density ( $\text{kg m}^{-3}$ ) ( $\text{m}^2 \text{s}^{-1}$ )			Ratio of turbulence spectrum density to wind energy spectrum density (%)		
		Frequency	Frequency	Frequency	Frequency	Frequency	Frequency
		1	2	3	1	2	3
8-14	5070	$1.7 \times 10^{-3}$	$8.4 \times 10^{-4}$	$2.7 \times 10^{-4}$	5.3	19.8	18.1
	4110	$1.8 \times 10^{-3}$	$8.4 \times 10^{-4}$	$2.3 \times 10^{-4}$	5.7	18.4	17.3
June	13150	$1.3 \times 10^{-3}$	$5.6 \times 10^{-4}$	$1.7 \times 10^{-4}$	5.5	19.3	18.7
2011	2190	$1.1 \times 10^{-3}$	$4.4 \times 10^{-4}$	$1.4 \times 10^{-4}$	2.0	6.7	8.9
	1110	$8.5 \times 10^{-4}$	$3.7 \times 10^{-4}$	$1.2 \times 10^{-4}$	1.0	5.4	19.7

in peak areas, which reflects that there are several disturbances in the rainstorm which occurred in the warm sector and there was no cold air at upper levels. The occurrence of the peaks may be because of the vertical movement of precipitation clouds.

**5.4 Spectrum characteristics of severe convective weather**

On 3 June 2012, hailstorms, possibly due to trough-line activities, occurred in Beijing, with more

than 20 mm of precipitation. Figure 9a shows the horizontal wind speed below the altitude of 5000 m during 3-5 June 2012. Figure 9b shows the wind energy spectrum and Fig. 9c shows the turbulence spectrum for this severe convective weather case.

In Fig. 9b, the spectrum is smooth and there are no peaks. The amplitude is four times bigger than in the summer rainstorm, and is close to that in cold windy weather. From 5070 to 3150 m, the spectrum

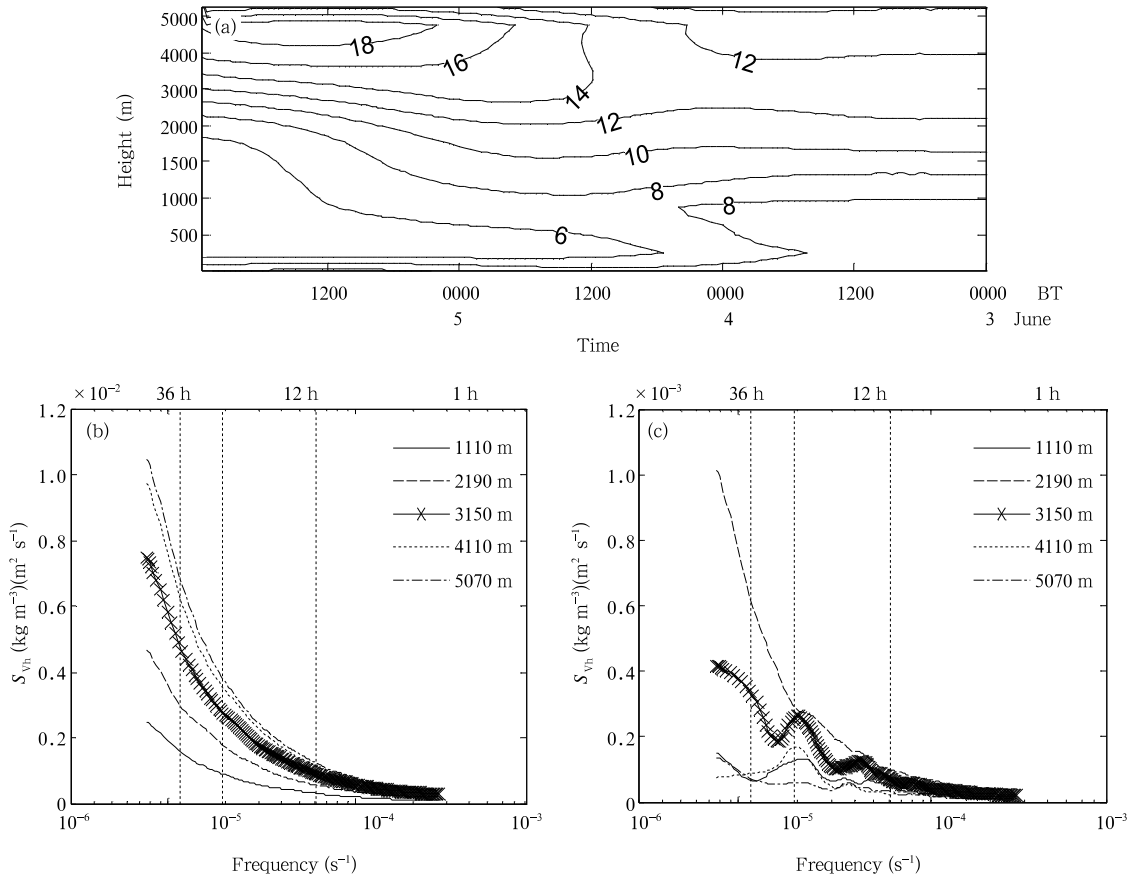


**Fig. 9.** As in Fig. 7, but for the severe convective weather case during 3-5 June 2012.

density decreases only a little, while it reduces rapidly below 3150 m, showing that the wind energy transmits faster at the lower level. The spectrum characteristics are similar to those of cold windy weather because the two cases are both related to a cold front. The spectrum of turbulence has two peaks at all the heights except 2190 m; one at a frequency of  $2 \times 10^{-5} \text{ s}^{-1}$  and the other at  $6 \times 10^{-5} \text{ s}^{-1}$ . These peaks occur at about 13 and 9 h. The amplitude of the peaks is stronger at low altitude. The maximum amplitude is at 3150 m and the minimum is at 5070 m, which shows that the turbulence is more vigorous at 3000 m. This may be because of the activity of the trough-line. The amplitude at 1110 m is larger than that at 5070 m, mainly because of the activity of turbulence in the warm sector.

Table 6 is a summary of the spectral density of horizontal wind at five heights in this severe convective weather case. The spectral density decreases with decreasing altitude. The amplitude of the spectrum at the same altitude and the same frequency in severe convective weather is larger than that in stable weather. The higher the frequency, the less the spectrum density, and the larger the turbulence spectrum density accounting for the proportion of the wind energy spectrum density, indicating that the energy in the high energy scale at low frequency transmits to the low energy scale at high frequency. In peak areas, the turbulence spectrum density accounting for the proportion of the wind energy spectrum density is larger than other areas, especially at 3150 and 2190 m. This may be because of the intense vertical movement

**Table 6.** Spectral density of horizontal wind at five heights in the case of severe convective weather

Sampling time	Height (m)	Wind energy spectrum density ( $\text{kg m}^{-3}$ ) ( $\text{m}^2 \text{ s}^{-1}$ )			Ratio of turbulence spectrum density to wind energy spectrum density (%)		
		Frequency	Frequency	Frequency	Frequency	Frequency	Frequency
		1	2	3	1	2	3
June 3 to 5, 2012	5070	$6.5 \times 10^{-3}$	$3.8 \times 10^{-3}$	$1.2 \times 10^{-3}$	0.4	1.0	2.6
	4110	$6.0 \times 10^{-3}$	$3.5 \times 10^{-3}$	$1.1 \times 10^{-3}$	0.1	1.5	2.6
	3150	$4.5 \times 10^{-3}$	$2.8 \times 10^{-3}$	$8.9 \times 10^{-4}$	1.7	7.7	8.9
	2190	$2.8 \times 10^{-3}$	$1.8 \times 10^{-3}$	$5.5 \times 10^{-4}$	9.8	20.9	5.5
	1110	$1.5 \times 10^{-3}$	$9.0 \times 10^{-4}$	$3.2 \times 10^{-4}$	2.4	3.0	3.2

at the middle level.

## 6. Summary and conclusions

In this study, spectral analysis of wind profiling radar observations at heights of 1–5 km has been made. The wind energy and turbulence spectrum in different weather conditions shows different characteristics, which are helpful to the analysis and research of weather systems.

Turbulence spectrum in stable weather conditions at high altitude is expressed in powers in the frequency range  $2 \times 10^{-5}$ – $10^{-3} \text{ s}^{-1}$ . The slope  $b$  is between  $-0.82$  and  $-1.04$ , indicating that the turbulence is in the transition zone from the energetic range to the inertial sub-range. Wind shear and convective activity may enhance the turbulence.

The peaks seen in the turbulence spectrum show the period of the weather system. Cold windy weather

appears at a period of 1.5 days in the turbulence spectrum, and the amplitude at 5 km is the largest. The wide-range summer rainstorm exhibits two or three peaks in the spectrum over 15–20 h. In the severe convective weather conditions there are two peaks at 13 and 9 h.

Compared with stable weather, the turbulence spectrum density accounting for the proportion of the wind energy spectrum density increases rapidly, especially in peak areas, in severe weather conditions.

## REFERENCES

- Atkinson, B. W., 1981: *Mesoscale Atmospheric Circulations*. Academic Press, 495 pp.
- Bian Jianchun, Qiao Jinsong, and Lu Daren, 2002: Laboratory for middle atmosphere and global environment observation. *Chinese J. Atmos. Sci.*, **26**, 474–480. (in Chinese)

- Bowne, N. E., and J. T. Ball, 1970: Observational comparison of rural and urban boundary layer turbulence. *J. Appl. Meteor.*, **9**, 862–873.
- Chellali, F., A. Khellaf, and B. Adel, 2010: Application of time-frequency representation in the study of the cyclical behavior of wind speed in Algeria: Wavelet transform. *Stochastic Environmental Research and Risk Assessment*, **24**, 1233–1239.
- Deng Chuang, Ruan Zheng, Wei Ming, et al., 2012: The evaluation of wind measurement accuracy by wind profile radar. *J. Appl. Meteor. Sci.*, **23**, 523–533. (in Chinese)
- Endlich, R. M., R. C. Singleton, and J. W. Kaufman, 1969: Spectral analysis of detailed vertical wind speed profiles. *J. Atmos. Sci.*, **26**, 1030–1041.
- Griffith, H. L., H. A. Panofsky, and I. van der Hoven., 1956: Power-spectrum analysis over large ranges of frequency. *J. Atmos. Sci.*, **13**, 279–282.
- Højstrup, J., 1981: A simple model for the adjustment of velocity spectra in unstable conditions downstream of an abrupt change in roughness and heat flux. *Bound.-Layer Meteor.*, **21**, 341–356.
- Kaimal, J. C., J. C. Wyngaard, Y. Izumi, et al, 1972: Spectral characteristics of surface layer turbulence. *Quart. J. Roy. Meteor. Soc.*, **98**, 563–589.
- , and J. J. Finnigan, 1994: *Atmospheric Boundary Layer Flows: Their Structure and Measurement*. Oxford University Press, 1–279.
- Kolmogorov, A. N., 1941a: The local structure of turbulence in incompressible viscous fluid for very large Reynolds number. *Math. Phys. Sci.*, **434**, 9–13.
- , 1941b: Dissipation of energy in the locally isotropic turbulence. *Math. Phys. Sci.*, **434**, 15–17.
- Liu Shuyuan, Zheng Yongguang, and Tao Zuyu, 2003: The analysis of the relationship between pulse of land heavy rain using wind profiler data. *J. Trop. Meteor.*, **19**, 285–290. (in Chinese)
- Liu Xiaohong and Hong Zhongxiang, 1996: A study of the structure of a strong wind event in the atmospheric boundary layer in Belting area. *Scientia Meteor. Sinica*, **20**, 223–228. (in Chinese)
- Luo Jianyuan and Zhu Ruizhao, 1993: The analysis of wind spectrum characteristics in surface layer in Badaling area of Beijing. *Acta Energiæ Solaris Sinica*, **14**, 279–287. (in Chinese)
- Panofsky, H. A., 1955: Meteorological applications of power—Spectrum analysis. *Bull. Amer. Meteor. Soc.*, **36**, 163–166.
- , D. Larko, R. Lipschutz, et al., 1982: Spectra of velocity components over complex terrain. *Quart. J. Roy. Meteor. Soc.*, **108**, 215–230.
- Sheng Peixuan, Mao Jietai, Li Jianguo, et al., 2003: *Atmospheric Physics*. Beijing University Press, Beijing, 227–228. (in Chinese)
- Sun Aidong and Xu Yumao, 1997: Spectral characteristic and multi-scale analysis of a wet cold front in boundary-layer atmosphere. *Scientia Atmos. Sinica*, **17**, 18–27. (in Chinese)
- Sun Jisun, He Na, Wang Guorong, et al., 2012: Preliminary analysis on synoptic configuration evolution and mechanism of a torrential rain occurring in Beijing on 21 July 2012. *Torrential Rain and Disasters*, **31**, 218–225. (in Chinese)
- Tian Yuji, Yang Qingshan, Yang Na, et al., 2011: Beijing meteorological tower statistical model of turbulent wind velocity spectrum. *Scientia Sinica (Technologica)*, **41**, 1460–1468. (in Chinese)
- Van der Hoven, I., 1957: Power spectrum of horizontal wind speed in the frequency range from 0.0007 to 900 cycles per hour. *J. Meteor.*, **14**, 160–164.
- Wang Hua, Sun Jisong, and Li Jin, 2007: A comparative analysis on two severe hail events in Beijing urban district in 2005. *Meteor. Mon.*, **33**, 49–56. (in Chinese)
- Wang Xinyan and Mao Jietai, 2004: The wavelet application in the research of mesoscale convective activity features. *J. Trop. Meteor.*, **20**, 549–560. (in Chinese)
- Wei Fengying and Zhang Ting, 2009: Frequency distribution of drought intensity in Northeast China and relevant circulation background. *Journal of Natural Disasters*, **18**, 1–7. (in Chinese)
- Yu Xiaoding, 2012: Investigation of Beijing extreme flooding event on 21 July 2012. *Meteor. Mon.*, **38**, 1313–1329. (in Chinese)
- Zhang Xiaoping, Lü Naiping, and Zhou Mingyu, 1987: The characteristics of vertical distribution of low-frequency spectra for horizontal wind velocity in the atmospheric boundary layer. *Chinese J. Atmos. Sci.*, **11**, 31–39. (in Chinese)
- Zhao Deshan, Wang Lizhi, and Hong Zhongxiang, 1982: Analysis on the structure of gust in boundary layer when a cold front passing. *Chinese J. Atmos. Sci.*, **6**, 324–332. (in Chinese)